



Trans. Nonferrous Met. Soc. China 34(2024) 3282-3294

Transactions of Nonferrous Metals Society of China

www.tnmsc.cn



# Microstructure and martensitic transformation in quaternary NiTiHfV alloy

Aleksandr V. SHUITCEV<sup>1</sup>, Yi REN<sup>1</sup>, Ze-zhong ZHANG<sup>1</sup>, Roman N. VASIN<sup>2</sup>, Bin SUN<sup>3</sup>, Li LI<sup>1</sup>, Yun-xiang TONG<sup>1</sup>

- 1. International Joint Laboratory of Advanced Nanomaterials of Heilongjiang Province,
- College of Materials Science and Chemical Engineering, Harbin Engineering University, Harbin 150001, China;
  - 2. Frank Laboratory of Neutron Physics, Joint Institute for Nuclear Research, 141980, Dubna, Russia;
    - Center of Testing and Analysis, College of Materials Science and Chemical Engineering, Harbin Engineering University, Harbin 150001, China

Received 31 March 2023; accepted 26 September 2023

**Abstract:** The effect of age hardening on the microstructure, martensitic transformation behavior, and shape memory properties of the (Ni<sub>50</sub>Ti<sub>30</sub>Hf<sub>20</sub>)<sub>95</sub>V<sub>5</sub> alloy was investigated by scanning electron microscopy, transmission electron microscopy, X-ray diffraction, differential scanning calorimetry, microhardness, and bending tests. The results demonstrate a significant influence of V addition on the microstructure of the alloy. V addition leads to the formation of a (Ni,V)<sub>2</sub>(Ti,Hf)-type Laves phase, which coexists with *B*19′ martensite at room temperature. Aging at 550 °C results in precipitation hardening due to the formation of nano-scale orthorhombic *H*-phase, with the peak hardness observed after 3 h of aging. The alloy at peak hardness state exhibits higher transformation strain and lower unrecovered strain compared to the solution-treated sample. The aged sample achieves a maximum transformation strain of 1.56% under 500 MPa.

Key words: shape memory alloys; NiTiHfV; H-phase; Laves phase; martensitic transformation

#### 1 Introduction

NiTiHf-based high-temperature shape memory alloys (HTSMAs) have emerged as the promising candidates for practical applications in various engineering fields, such as automotive, aerospace, and nuclear energy, within the temperature range of 100–300 °C [1,2]. These alloys possess superior functional properties, including shape memory effect (SME), superelastic behavior, and significant work outputs resulting from reversible thermoelastic martensitic transformation (MT) [3]. However, compared to binary NiTi alloys, ternary NiTiHf alloys exhibit inferior shape recovery

properties due to their relatively low critical stress for dislocation slip [4,5]. Our previous studies suggested that this low critical stress for dislocation slip arises from the large volume effect of MT and the incapability of alloy matrix to elastically accommodate the stress during crystallographic rearrangement [6,7].

To enhance the recovery strain of NiTi-based SMAs through the increase of the dislocation slip stress of matrix, several strategies have been explored, including grain refinement, precipitation hardening and quaternary alloying. Grain refinement through severe plastic deformation is a promising strengthening method for NiTi-based alloys [8–12]; however, its commercial application

is limited due to the restricted ductility of NiTiHf based alloys.

Another potential approach is precipitation hardening, which has shown positive effects on the strain recovery properties of Ni-rich NiTiHf alloys. Previous studies have identified the formation of coherent nano-sized precipitates, known as the face-centered orthorhombic phase or *H*-phase, in Ni-rich Ni<sub>50.3</sub>Ti<sub>29.7</sub>Hf<sub>20</sub> alloys aged at 550 °C for 3 h [13–17]. These precipitates significantly impact MT temperatures and improve the strain recovery properties of Ni-rich NiTiHf alloys. For example, Ni<sub>50.3</sub>Ti<sub>29.7</sub>Hf<sub>20</sub> alloy aged at 550 °C for 3 h exhibits near-perfect high-temperature superelastic behavior with a fully recoverable strain of 4% [14].

Quaternary alloying has also proven effective in strengthening the NiTiHf matrix. Various alloying elements, including Nb [18], Ta [19], Sc [20,21], Y [22], Ag and Sn [23], Al [24], Cu [25-28], Pd [29,30], and Zr [31,32] have been added to NiTiHf alloys. These alloying elements exhibit different effects on the transformation temperatures (TTs) and grain size of NiTiHf alloys, as well as on their strength and strain recovery properties. For example, all of the above-mentioned elements except Zr reduce the TTs. Addition of Al reduces TTs at a rate of 100 °C/at.% in Ni<sub>50</sub>Ti<sub>30-x</sub>Hf<sub>20</sub>Al<sub>x</sub> alloys [24], while the alloying of Y has an insignificant effect on TTs with a rate of 1–1.5 °C/at.% [22]. The role of Zr in NiTiHf matrix is more complicated. Depending on Zr content, the increasing of TT rate varies from 6-7 to 50 °C/at.% in  $Ni_{50}Ti_{38-x}Hf_{12}Zr_x$  alloys [31]. The additions of Nb and Ta improve the workability of NiTiHf alloys by forming soft  $\beta$ -Nb and Ta-rich phases, respectively [18,19]. The additions of Y and Sc reduce the grain size of NiTiHf matrix by forming Y- and Sc-rich precipitates distributed along grain boundaries [20-22]. Quaternary elements can significantly enhance the strength of the alloy matrix, positively affecting the strain recovery properties. For example, a high-strength single crystal Ti<sub>29.7</sub>Ni<sub>45.3</sub>Hf<sub>20</sub>Pd<sub>5</sub>, with [111] orientation, exhibits perfect superelastic behavior and a fully recoverable strain of 4.2% [33].

It has been reported that the addition of a small amount of V into binary NiTi alloys improves strain recovery properties due to solution strengthening effect [34], while lager amount of V leads to the

appearance of soft  $\beta$ -V phase [35,36]. The above results indicate that the addition of V into NiTiHf alloys may enhance the functional properties through solution strengthening and precipitation strengthening. However, the influence of V on the microstructure and functional properties of ternary NiTiHf alloys remains unknown. To address this gap, we added V to Ni<sub>50</sub>Ti<sub>30</sub>Hf<sub>20</sub> alloy and investigated the evolution of microstructure and functional properties with aging in (Ni<sub>50</sub>Ti<sub>30</sub>Hf<sub>20</sub>)<sub>95</sub>-V<sub>5</sub> HTSMAs.

## 2 Experimental

A 70 g  $(Ni_{50}Ti_{30}Hf_{20})_{95}V_5$  (at.%) alloy ingot was prepared by arc melting at a high-purity argon atmosphere with high purity raw materials. Hereafter, this composition is expressed as NiTiHfV. The ingot underwent eight remelting cycles, with flipping after each melting step to ensure composition homogeneity. Prior to melting the NiTiHfV alloy, a pure Ti button was melted as an oxygen-getter. After melting, the ingot was sealed in a vacuum inside a quartz tube and subjected to solution treatment at 900 °C for 4 h, followed by water quenching. Samples with a thickness of approximately 1 mm were prepared by electro-spark cutting from the solution-treated alloy. The sample surfaces were ground to remove cutting marks. Subsequently, some samples were aged at 550 °C for different durations ranging from 0.1 to 10 h. Aging with durations longer than 1 h was performed in evacuated quartz tubes to prevent oxidation. Aging at 550 °C has been reported to yield the best strain recovery properties in NiTiHfbased alloys, as mentioned in Refs. [11,12].

The phase transformation behavior was investigated by differential scanning calorimetry (DSC) using a Perkin Elmer diamond instrument with heating and cooling rates of 20 °C/min. X-ray diffraction (XRD) was carried out on a PANalytical Xpert'pro diffractometer using Cu  $K_{\alpha}$  radiation by step-scanning in the  $2\theta$  range of  $25^{\circ}-110^{\circ}$ . The MAUD software package [37] was used for the analysis of XRD data.

Microstructure characterization was conducted using scanning electron microscope (SEM) equipped with energy dispersive spectroscope (EDS). SEM images were acquired in backscattered electron (BSE) mode. The transmission electron

microscopy (TEM) observations were performed using a Talos 200FX G2 electron microscope operated at 200 kV with a double-tilt stage. The foils for TEM observations were prepared by mechanical grinding of the samples to a thickness of 50  $\mu$ m, followed by low-temperature ion-milling.

Shape memory effect (SME) measurements were conducted using a dynamic mechanical analyzer (DMA 850) from TA Instruments equipped with a three-point bending clamp. The distance between the two supporting pins was 20 mm. The sample dimensions for SME determination were  $30 \text{ mm} \times 0.9 \text{ mm} \times 0.5 \text{ mm}$ . A constant flexural stress was initially applied to the midpoint of the sample, and then the sample was cooled and heated at a rate of 5 °C/min to measure the flexural strain during MT. After each cycle, a higher flexural stress was applied. Microhardness measurements were carried out on a HVS-1000 Vickers microhardness tester. Samples for microhardness testing were mechanically polished. To avoid the indentation size effect [38], the load on the indenter was chosen to be 200 g with a loading duration of 10 s. The data reported are the average of at least 10 points of each sample measured.

# 3 Results and discussion

### 3.1 Age hardening behavior

The evolution of microhardness as a function of aging time for NiTiHfV alloy aged at 550 °C is illustrated in Fig. 1. The as-cast sample exhibits a microhardness value estimated at HV (432±3). After solution treatment, the microhardness value decreases to HV (417±7) and reaches a peak of HV (535±5) after 3 h of aging at 550 °C. Subsequent aging results in a continuous decrease in microhardness to HV (520±5) after 10 h. This evolution of microhardness with aging duration confirms the classical behavior of precipitation hardening. Similar results are observed  $Ni_{50}Ti_{30}Hf_{20}$ [39],  $Ni_{50.3}Ti_{29.7}Hf_{20}$ [40] Ni<sub>50.8</sub>Ti<sub>34.2</sub>Zr<sub>15</sub> [41] alloys aged at 550 °C, although the peak in hardness appears at different aging duration due to the different Ni contents in alloy matrix. For the NiTiHfV alloy, aging at 550 °C results in a maximum increase in hardness of approximately HV 117. By comparison, hardness increases in  $Ni_{50.3}Ti_{34.}7Hf_{15}$  $Ni_{50}Ti_{30}Hf_{20}$  [39], and  $Ni_{50.8}Ti_{34.2}Zr_{15}$  [41] alloys are reported to be approximately HV 78, HV 125, and HV 169, respectively.

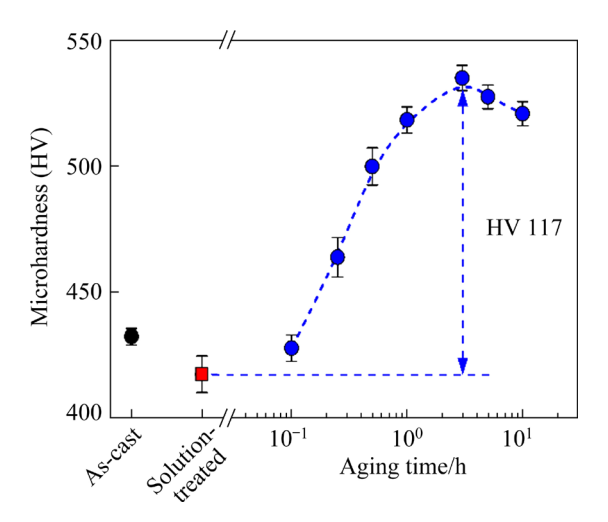
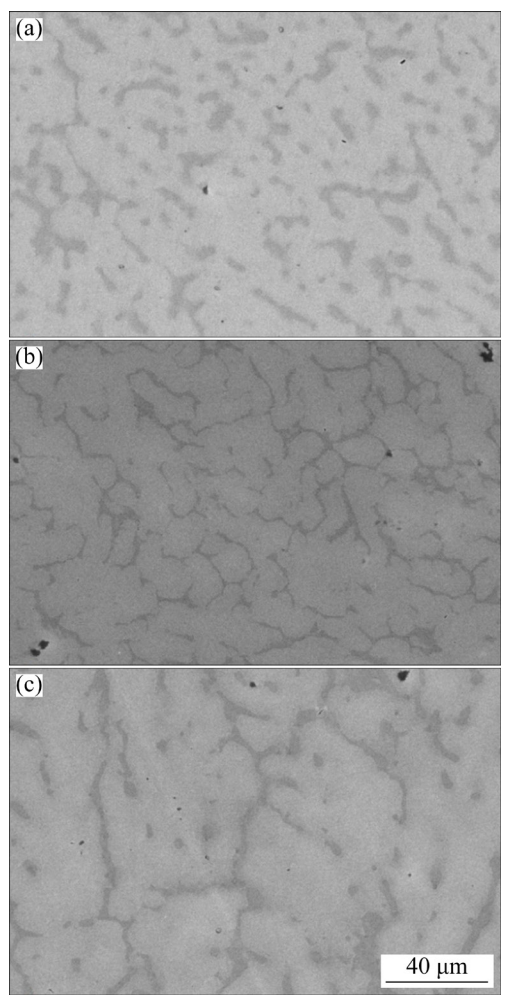


Fig. 1 Evolution of microhardness as function of aging time for NiTiHfV alloy aged at  $550 \, ^{\circ}\mathrm{C}$ 

#### 3.2 Microstructure evolution

Figures 2(a-c) display the backscattered electron (BSE) micrographs of the as-cast, solutiontreated, and aged (550 °C for 3 h) NiTiHfV samples, respectively, revealing the presence of two distinguishable phases. The first phase corresponds to the matrix, appearing as light grey in color. The second phase consists of inclusions, exhibiting a dark grey color and primarily distributed along the grain boundaries of the matrix. The evolution of surface area fraction and size of the second phase is presented in Fig. 3. For the as-cast sample, the surface area fraction of the second phase is estimated to be (27.6±4.0)%. After solution treatment, the surface area fraction is reduced to (16.8±2.5)% and does not change after aging at 550 °C for 3 h. The widths of the second phase inclusions are calculated to be  $(5.4\pm1.6)$ ,  $(2.5\pm0.8)$ and (5.4±0.8) µm for the as-cast, solution treated and aged samples, respectively.

The chemical compositions of the matrix and second phase of NiTiHfV alloy after different heat treatments were measured by EDS analysis and are listed in Table 1. Unfortunately, the quaternary Ni-Ti-Hf-V phase diagram is not available, making the direct identification of the second phase a challenging task. However, based on the composition and element ratios, it is proposed that the second phase in the studied alloy corresponds to a (Ni,V)<sub>2</sub>(Ti,Hf)-type Laves phase [43].



**Fig. 2** BSE micrographs of as-cast sample (a), solution-treated sample (b) and sample aged at 550 °C for 3 h (c)

The decrease in the area fraction of the Laves phase is likely attributed to an increase in the solubility of V into NiTiHf matrix at 900 °C. This assumption is supported by the results presented in Table 1, where the V content in the matrix of the solution-treated sample increases to approximately 4.4 at.% compared to approximately 3 at.% in the as-cast and aged samples. Moreover, the reduction in width of the second phase further supports this assumption. The solubility of V in binary NiTi matrix at 900 °C is estimated to be ~7 at.% [44,45].

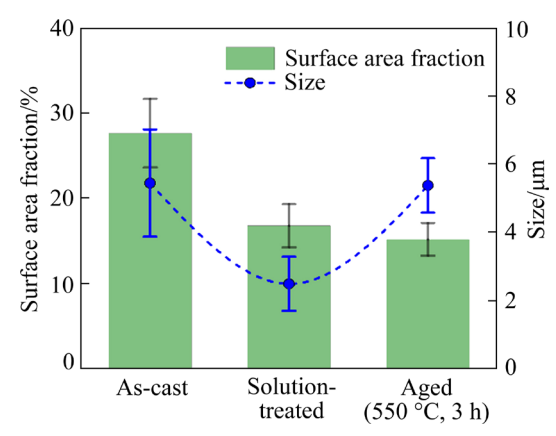


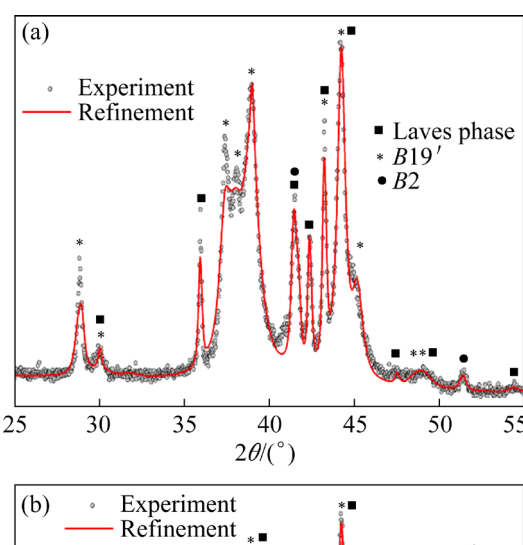
Fig. 3 Evolution of surface area fraction and size of second phase in NiTiHfV samples

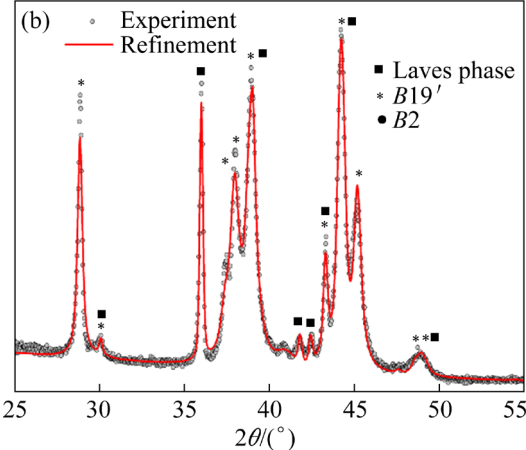
The changes in the area fraction and width of (Ni,V)<sub>2</sub>(Ti,Hf) phase result in alterations in the strength of the alloy. For instance, the microhardness in NiTiHfV alloy decreases from HV (432±3) to HV (417±7) for the as-cast and solution-treated samples, respectively.

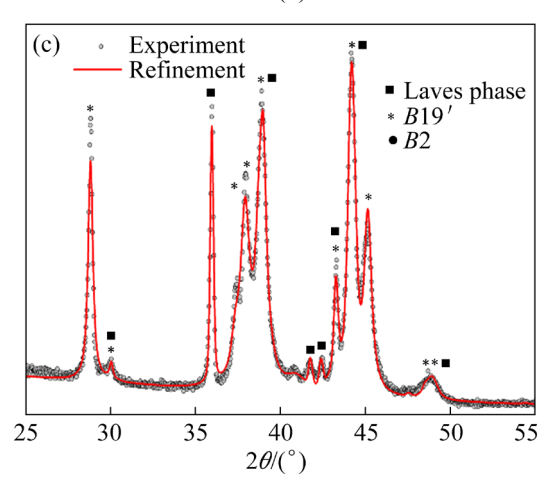
To shed light on the structure of NiTiHfV alloy, XRD analysis was carried out. Figure 4 shows the room-temperature XRD patterns of differently treated NiTiHfV samples. One of the phases observed is monoclinic B19' martensite, which contributes to the multiple overlapped diffraction peaks of the pattern. In this case, phase or Rietveld analysis could not be readily made. Therefore, Le Bail refinement of the measured diffraction patterns was used to determine the crystallographic parameters of the phases [46]. All the observed diffraction peaks are properly described during the refinement with one exception. The diffraction patterns of the solution-treated and aged samples show an additional diffraction peak at a scattering angle of  $2\theta \approx 41^{\circ}$ , corresponding to lattice spacing of ~2.2 Å. This closely corresponds to the position of most intensive X-ray diffraction peaks (426) and (040) of H-phase [17]. The intensity of the additional diffraction peak is very small in the pattern of the solution-treated sample but increases

Table 1 Chemical compositions of matrix and second phase for NiTiHfV alloy at different states

Alloy	Composition of matrix/at.%				Composition of second phase/at.%			
	Ni	Ti	Hf	V	Ni	Ti	Hf	V
As-cast	49.59	29.20	18.13	3.08	33.02	25.13	13.64	28.21
Solution-treated	48.19	31.01	16.40	4.41	33.32	24.38	13.19	29.11
Aged (550 °C, 3 h)	50.01	28.09	18.99	2.91	32.84	24.81	13.61	28.75







**Fig. 4** Room-temperature XRD patterns and corresponding Le Bail refinement fits of as-cast sample (a), solution-treated sample (b) and sample aged at 550 °C for 3 h (c)

by  $\sim 10$  times in that of the aged sample. This is possibly related to the precipitation and growth of H-phase particles. The diffraction peaks of austenitic B2 phase (space group Pm3m) are only distinguishable for the as-cast sample. Thus, the main phases in NiTiHfV samples at room temperature are monoclinic B19' martensite (space

group P21/m) and Laves phase (space group P6/mmc).

The crystal lattice parameters of different phases in NiTiHfV samples are listed in Table 2. It is seen that heat treatment barely affects the lattice parameters of B19' martensite and Laves phase. Moreover, lattice parameters of B19' martensite are close to those previously reported for Ni<sub>50.3</sub>Ti<sub>29.7</sub>Hf<sub>20</sub> alloy, i.e., a=3.053 Å, b=4.065 Å, c=4.871 Å and  $\beta$ =103.1° [6]. Therefore, the addition of 5 at.% V to NiTiHf does not significantly alter the lattice parameters. Lattice parameters of Laves phase are consistent with those of hexagonal Laves phase (Ni,V)<sub>2</sub>(Hf,Ti) reported in Ref. [43], i.e., a=5.024 Å and c=8.194 Å, considering the compositional difference between this phase in the studied samples (Table 1) and that defined in Ref. [43].

**Table 2** Lattice parameters of various phases in NiTiHfV alloy

Phase	Parameter	As-	Solution-	Aged	
		cast	treated	(550 °C, 3 h)	
B19' (P21/m)	a/Å	3.047	3.051	3.048	
	b/Å	4.094	4.084	4.083	
	$c/\mathrm{\AA}$	4.852	4.860	4.853	
	β/(°)	102.6	102.6	102.7	
B2 (Pm3m)	a/Å	3.080	_	-	
Laves phase (P6/mmc)	a/Å	4.997	4.991	5.001	
	c/Å	8.188	8.185	8.192	

Figure 5 shows the TEM micrographs and the corresponding selected area electron diffraction (SAED) patterns of the solution-treated NiTiHfV alloy. The martensitic variants characterized by the lath-like morphology are well-defined (Fig. 5(a)). The SAED pattern in Fig. 5(b) shows that martensite substructure is mainly (001) compound twin. The variants are related to the (111) type I twin, which is confirmed by the pattern shown in Fig. 5(b) taken from the interface of variants in Fig. 5(a) marked with circle. The (111) type I martensitic variants were previously reported for TiB/NiTiHf composite [47,48]. No precipitates of *H*-phase are identified in the martensitic matrix.

Bright field image of the second phase inclusion in the solution-treated NiTiHfV alloy is presented in Fig. 5(c). SAED pattern in Fig. 5(d) taken from the circled area in Fig. 5(c) confirms

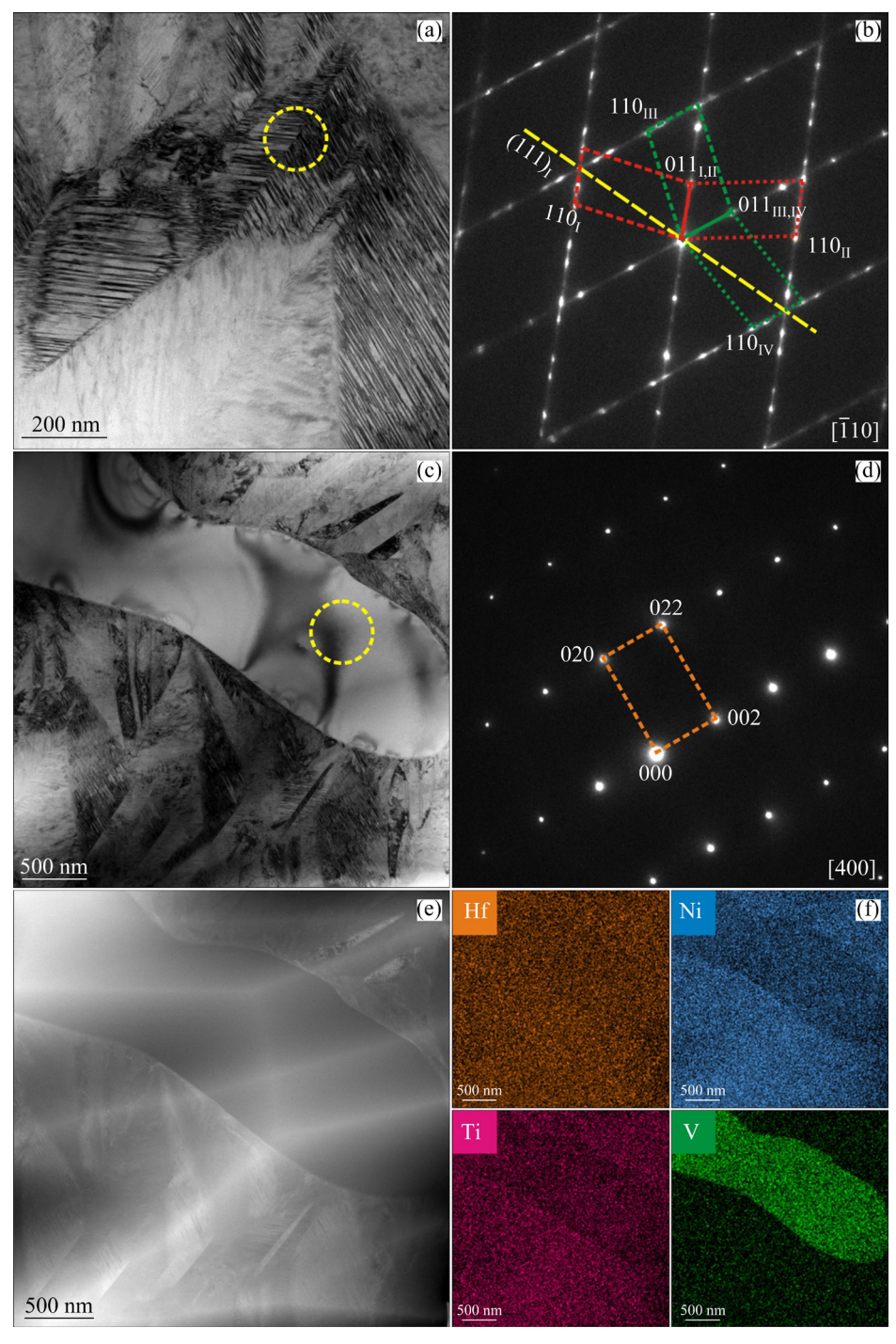


**Fig. 5** Bright field TEM micrographs (a, c) and corresponding SAED patterns (b, d) of martensite matrix (a, b) and inclusion of second phase (c, d) in solution-treated NiTiHfV alloy; STEM-HAADF image (e) of inclusion of second phase and corresponding EDS mappings (f) for Hf, Ni, Ti and V

that the inclusion is the Laves phase. Figure 5(e) shows a STEM-HAADF TEM micrograph and Fig. 5(f) shows the elemental mapping images for Hf, Ni, Ti and V. It can be observed that the Laves phase is much richer in V and poorer in Ni and Ti compared to the matrix. The difference in Hf content is relatively small between the two phases.

This aligns well with the composition measured by EDS, as given in Table 1.

The TEM micrograph and the corresponding SAED pattern of the sample aged at 550 °C for 3 h are shown in Fig. 6. Clear evidence of *H*-phase precipitates can be observed in Fig. 6(a) and is confirmed by the corresponding SAED pattern in

Fig. 6(b). The size of H-phase precipitates is estimated to be (28.4±2.1) nm in length (long axis) and  $(11.2\pm0.8)$  nm in width (short axis) (Fig. 7(a)). It is important to note that aging at 550 °C for 3 h leads to the attainment of peak hardness, reaching a value of HV (535±5) (Fig. 1). The peak hardness typically signifies a transition in the interaction mechanism between the precipitates dislocations. Initially, the dominant mechanism is dislocation cutting, but as the precipitates reach a critical size, the coherency between the matrix and precipitates is broken down, and dislocations are compelled to loop around the precipitates instead of being cut through by them (known as the Orowan mechanism). Figure 7(b) shows the evolution of critical size of H-phase which corresponds to the peak hardness as a function of aging temperature for NiTiHf-based alloys. Previous studies have reported the critical size of the H-phase to be approximately (31.6±2.5) nm in length (12.6±0.8) nm in width for Ni<sub>50</sub>Ti<sub>30</sub>Hf<sub>20</sub> alloy aged

at 550 °C for 10 h [49]. The critical size of the *H*-phase observed in our study for the NiTiHfV alloy aligns well with these findings reported.

The bright field, dark field, STEM-HAADF and the elemental mapping images for Hf, Ni, Ti and V of the second phase of aged NiTiHfV alloy are shown in Figs. 8(a-d). The Laves phase clearly exhibits distinguishable new inclusions. These inclusions are characterized by a higher Ti content and lower V and Hf content compared to the surrounding Laves phase. The difference in Ni content between the two phases is relatively small. EDS analysis estimates the composition of the new inclusions as follows: 49.0 at.% Ti, 35.5 at.% Ni, 9.9 at.% Hf, and 5.6 at.% V. The SAED patterns of the inclusion phase are shown in Figs. 8(e-h) along its  $[00\overline{1}]$ ,  $[1\overline{14}]$ ,  $[\overline{1}11]$ , and  $[11\overline{6}]$  zone axes, respectively. Combining the EDS and SAED results indicates that this phase is the Ti<sub>2</sub>Ni-type phase with a cubic structure (space group: Fd3m). The lattice parameter is estimated to be 11.428 Å,

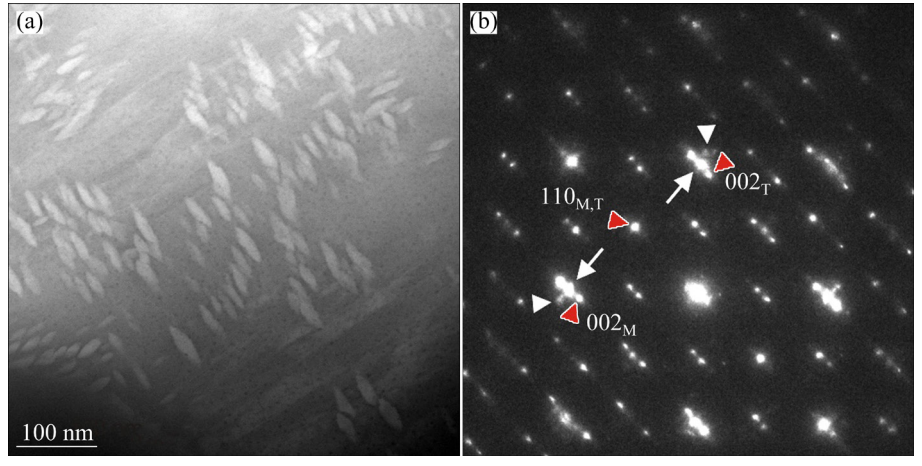


Fig. 6 TEM micrograph (a) and corresponding SAED pattern (b) of NiTiHfV alloy aged at 550 °C for 3 h

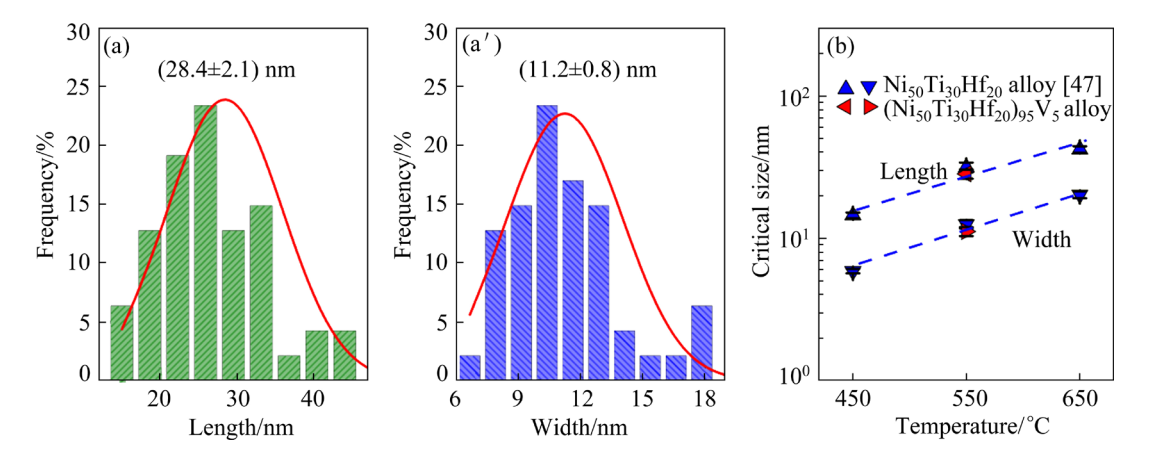
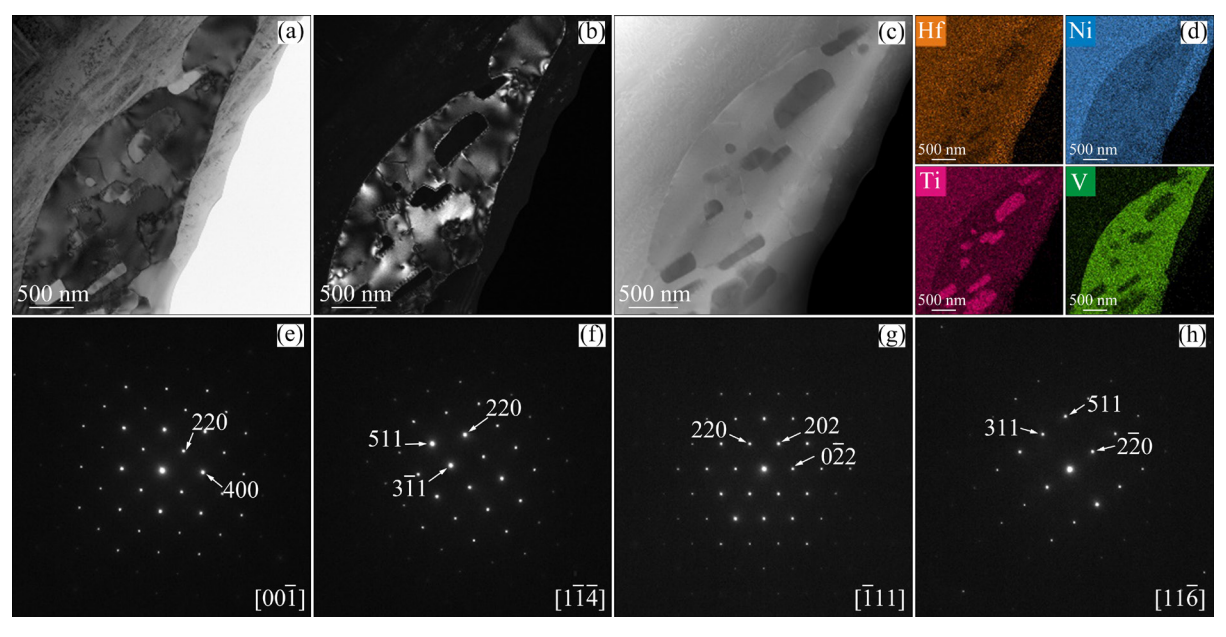


Fig. 7 Histogram of particle size distribution of *H*-phase in NiTiHfV alloy after aging at 550 °C for 3 h (a, a'), and comparison of critical size of *H*-phase corresponding to peak strength (b)

which closely aligns with the  $Ti_2Ni$  phase observed in binary NiTi alloys (11.3193 Å) [50]. Notably, the absence of the  $Ti_2Ni$ -type phase in the solution-treated sample suggests its formation during aging as a result of the decomposition of the Laves phase of  $(Ni,V)_2(Hf,Ti)$ . The presence of  $Ti_2Ni$ -type inclusions within the Laves phase further substantiates this assumption.

#### 3.3 Evolution of transformation temperatures

The DSC curves for the NiTiHfV alloy aged at 550 °C for various durations are presented in Fig. 9(a). During heating and cooling cycles, single endo- and exothermal peaks are observed in all cases, indicating a single-step transformation corresponding to reversible  $B2 \leftrightarrow B19$  martensitic transformation in NiTiHf-based alloys. Figure 9(b)



**Fig. 8** TEM bright field (a), dark field (b) and STEM-HAADF (c) images of Laves phase with inclusions of  $Ti_2Ni$ -type phase and corresponding EDS mapping (d) for Hf, Ni, Ti and V; SAED patterns of  $Ti_2Ni$ -type phase taken along  $[00\overline{1}]$  (e),  $[1\overline{14}]$  (f),  $[\overline{1}11]$  (g), and  $[11\overline{6}]$  (h) zone axes

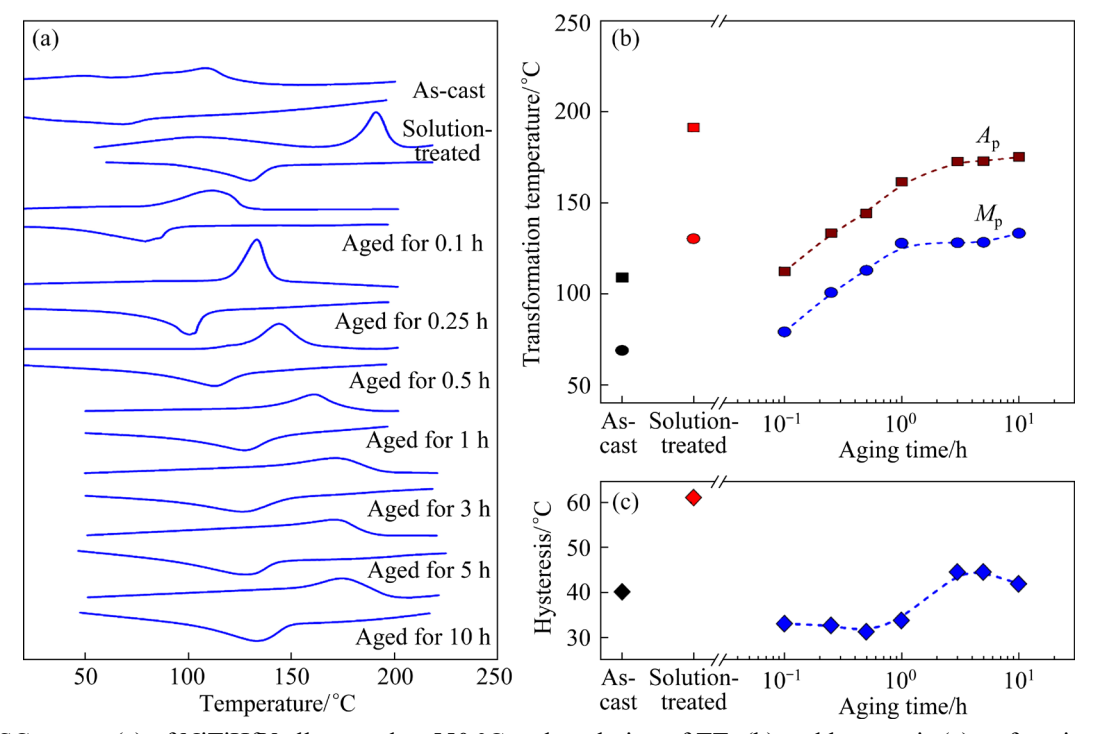


Fig. 9 DSC curves (a) of NiTiHfV alloy aged at 550 °C and evolution of TTs (b) and hysteresis (c) as function of aging duration

displays the martensitic  $(M_p)$  and austenitic  $(A_p)$  transformation peak temperatures as a function of aging duration. The as-cast sample exhibits the lowest  $M_p$  temperature, approximately 69 °C, while the highest  $M_p$  temperature of 130 °C is observed in the solution-treated sample. Short-duration aging of 6 min at 550 °C results in decreasing of  $M_p$  temperature to ~79 °C. Subsequent continuous aging leads to an increase in TTs.  $M_p$  and  $A_p$  temperatures are stabilized after 1 h aging at ~128 °C and 3 h at ~173 °C, respectively.

The difference in transformation temperatures between the solution-treated and as-cast samples can be attributed to the varying V contents in the alloy matrix (see Table 1). Further changes in transformation temperatures after aging primarily due to the formation of H-phase precipitates (Fig. 6(a)). This behavior of TTs during precipitation hardening is typical for NiTiHf-based alloys. The decrease in TTs is associated with a higher volume fraction of nanometric precipitates and a smaller interparticle distance, which suppresses MT. Consequently, a greater undercooling is required for the initiation of the martensitic shift. The increase in TTs after aging is correlated with the change in Ni content within the alloy matrix caused by H-phase precipitation. The decrease and increase of TTs are commonly referred to as mechanical and chemical effects, respectively [4].

The evolution of transformation hysteresis  $(A_p-M_p)$  is shown in Fig. 9(c). The solution-treated sample exhibits the largest hysteresis, 60 °C approximately. Aging at 550 °C for up to 1 h reduces the hysteresis to 30 °C. Further increase in aging duration enhances the transformation hysteresis up to ~40 °C. The significant increase in hysteresis is associated with the higher V content in the NiTiHf matrix resulting from the solution treatment. Similar effect has been observed for ternary NiTiNb alloys [51], where an increase in Nb content in the NiTi matrix leads to an increase in transformation hysteresis. The decrease of hysteresis upon aging is attributed to the formation of fine nano-scale H-phase precipitates. These fine precipitates improve the resistance to the defect formation [52], increase the elastic energy storage of an alloy matrix [53] and do not interfere with the growth of wide martensite variants during MT, resulting in lower transformation hysteresis. Further increase in aging duration leads to a rise in hysteresis due to larger precipitates that hinder the growth of martensite variants within the space between precipitates. Consequently, more energy is dissipated during MT, leading to an increase in the transformation hysteresis [52].

The observed increase in hysteresis during the aging process at 550 °C for the NiTiHfV alloy aligns with previous findings for Ni<sub>50</sub>Ti<sub>30</sub>Hf<sub>20</sub> alloy [49]. However, unlike the continuous increase in hysteresis observed in Ni<sub>50</sub>Ti<sub>30</sub>Hf<sub>20</sub> alloy, the NiTiHfV alloy exhibits a leap increase in thermal hysteresis. This leap can be attributed to the decomposition of the Laves phase (Ni,V)<sub>2</sub>(Hf,Ti) and the subsequent formation of the Ti<sub>2</sub>Ni-type phase. This phase transformation leads to a redistribution of V atoms among the *B*2, Ti<sub>2</sub>Ni-type, and Laves phases. Consequently, this structural evolution contributes to the significant rise in thermal hysteresis observed in the NiTiHfV alloy.

#### 3.4 Shape memory property

Figures 10(a, b) depict the strain-temperature curves for the solution-treated and aged samples of NiTiHfV alloy, respectively. It is evident that the aged sample exhibits larger transformation strain at all stress levels than the solution-treated sample. Transformation and unrecovered strains for both samples as well as the relationship between transformation strain and applied stress are presented in Fig. 10(c), revealing a continuous increase in transformation strain with the rise in applied stress. The transformation strains are found to be 0.7% and 1.2% at 400 MPa for the solution-treated and aged samples, respectively. For each applied stress, the unrecovered strain levels were measured at temperatures above  $A_{\rm f}$  (the finish temperature of reverse MT) by calculating the difference in strain between the heating and cooling curves. The experimental results show unrecovered strains of 0.11% and 0.02% at 400 MPa for the solution-treated and aged samples, respectively. The significant reduction in unrecovered strain in the aged sample is attributed to the precipitation hardening of H-phase. The presence of nano-scale H-phase precipitates acts as dislocation barriers, impeding the movement of dislocations and thereby increasing the dislocation slip stresses. This enhancement in dislocation slip stresses contributes to a more efficient and reversible strain recovery behavior in the aged sample.

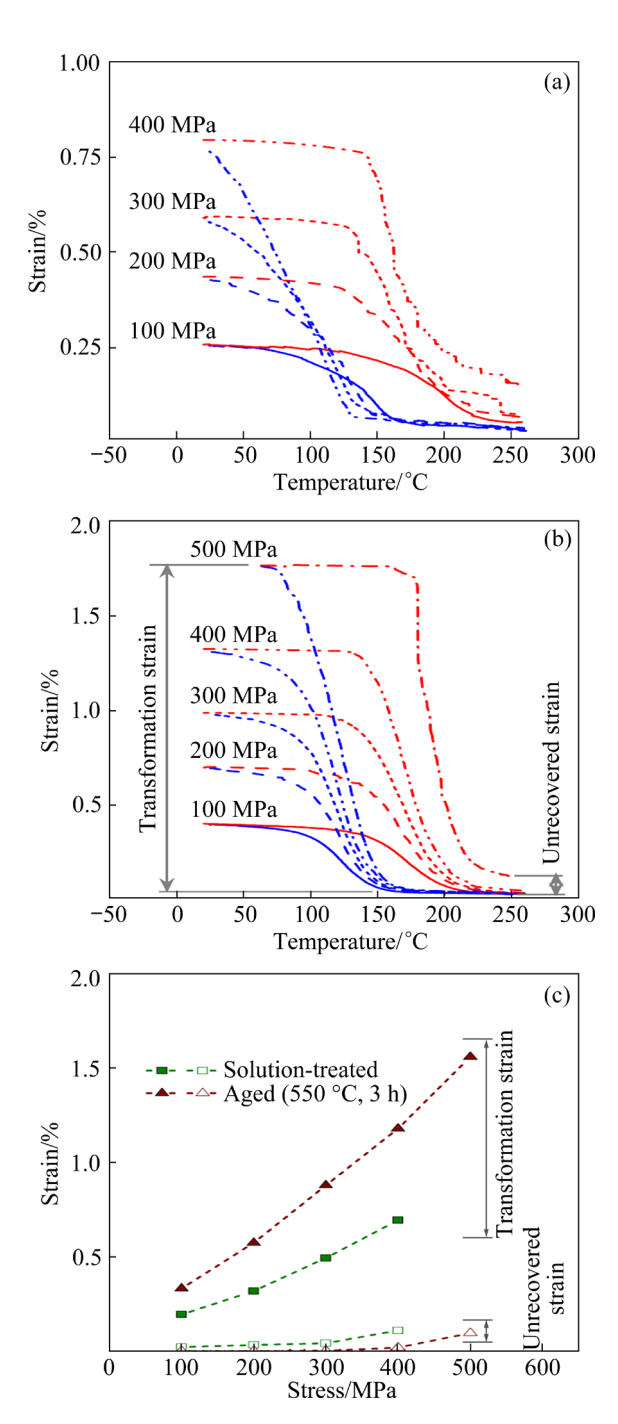


Fig. 10 Strain—temperature curves of solution-treated (a) and aged samples (b) of NiTiHfV alloy and effect of applied stress on transformation and unrecovered strains (c)

In the aged sample, a transformation strain of 1.56% and an unrecovered strain of 0.1% are achieved at 500 MPa. It is worth noting that the maximum transformation strain obtained in this study is lower than that observed in other alloys, such as Ni<sub>50.3</sub>Ti<sub>29.7</sub>Hf<sub>20</sub> (4.7% at 500 MPa under tension) [54], Ni<sub>45.3</sub>Ti<sub>29.7</sub>Hf<sub>20</sub>Pd<sub>5</sub> (3.3% at 1000 MPa

under compression) [30], and Ni<sub>45.3</sub>Ti<sub>29.7</sub>Hf<sub>20</sub>Cu<sub>5</sub> (2% at 500 MPa under compression) [55].

However, these comparisons should interpreted with caution due to several factors. Firstly, the current samples exhibit incomplete martensite reorientation/detwinning under applied which suggests that stress, the transformation strain may not have reached its saturation point. Furthermore, the experimental scheme used (e.g., tension, compression, torsion, bending) can significantly influence the observed transformation strain due to unique crystallography of martensitic transformation. Additionally, the presence of the (Ni,V)<sub>2</sub>(Ti,Hf)-type Laves phase in the studied alloy, with a significant volume fraction, can contribute to the lower transformation strain values. The Laves phase does not actively participate in the MT process, which can affect the overall strain behavior of the alloy.

The findings of previous research [53] have clearly demonstrated that the presence of H-phase in Ni<sub>50</sub>Ti<sub>30</sub>Hf<sub>20</sub> alloy results in a reduction of unrecovered strain, but it also leads to a decrease in transformation strain. This effect is likely attributed to a decline in the interface mobility between martensite and austenite due to the formation of H-phase precipitates. However, in the case of NiTiHfV alloy, the formation of *H*-phase contributes to an increase in transformation strain in the aged sample when compared to the solution-treated one, despite the higher proportion of the secondary phase. This suggests that the redistribution of V atoms between the matrix and secondary phase may enhance the mobility of the martensite/austenite interface.

#### 4 Conclusions

- (1) Age hardening behavior is observed during aging at 550 °C, with a peak microhardness of HV (535±5) achieved after 3 h of aging.
- (2) Apart from the matrix, the NiTiHfV alloy exhibits the presence of (Ni,V)<sub>2</sub>(Ti,Hf)-type Laves phase. The absence of precipitation is confirmed in the solution-treated sample, while aging at 550 °C for 3 h leads to the precipitation of *H*-phase, as confirmed through TEM observations.
- (3) Transformation temperatures experience a sharp reduction with short-duration aging at 550 °C, followed by a continuous increase with aging time

due to the formation of *H*-phase precipitates.

(4) *H*-phase precipitation strengthening significantly improves the shape memory effect of the alloy. The unrecovered strain decreases from 0.11% to 0.02% at the stress of 400 MPa during three-point bending thermal cycling experiments for the solution-treated and 3 h aged samples at 550 °C, respectively. Moreover, the aged sample exhibits a maximum recovered strain of 1.46% at the stress of 500 MPa.

#### CRediT authorship contribution statement

Aleksandr V. SHUITCEV: Conceptualization, Investigation, Writing – Original draft, Writing – Review & editing, Funding acquisition, Project administration; Yi REN: Investigation; Ze-zhong ZHANG: Investigation; Roman N. VASIN: Methodology, Investigation, Formal analysis, Writing – Review & editing; Bin SUN: Investigation; Li LI: Conceptualization; Yun-xiang TONG: Conceptualization, Writing – Review & editing, Supervision.

#### **Declaration of competing interest**

We declare that we have no financial and personal relationships with other people or organizations that can inappropriately influence our work, and there is no professional or other personal interest of any nature or kind in any product, service and/or company that could be construted as influencing the position presented in, or the review of, the manuscript entitled.

#### Acknowledgments

This study was supported by the National Natural Science Foundation of China (Nos. 52201207, 52271169).

#### References

- [1] MA J, KARAMAN I, NOEBE R D. High temperature shape memory alloys [J]. International Materials Reviews, 2010, 55: 257–315.
- [2] TONG Yun-xiang, SHUITCEV A V, ZHENG Yu-feng. Recent development of TiNi-based shape memory alloys with high cycle stability and high transformation temperature [J]. Advanced Engineering Materials, 2012, 22: 1900496.
- [3] OTSUKA K, REN X. Physical metallurgy of Ti-Ni-based shape memory alloys [J]. Progress in Materials Science, 2005, 50: 511-678.
- [4] EVIRGEN A, KARAMAN I, SANTAMARTA R, PONS J, NOEBE R D. Microstructural characterization and shape memory characteristics of the Ni<sub>50.3</sub>Ti<sub>34.7</sub>Hf<sub>15</sub> shape memory alloy [J]. Acta Materialia, 2015, 83: 48–60.

- [5] WANG Y Q, ZHENG Y F, CAI W, ZHAO L C. The tensile behavior of Ti<sub>36</sub>Ni<sub>49</sub>Hf<sub>15</sub> high temperature shape memory alloy [J]. Scripta Materialia, 1999, 40: 1327–1331.
- [6] SHUITCEV A V, VASIN R N, FAN X M, BALAGUROV A M, BOBRIKOV I A, LI L, GOLOVIN I S, TONG Y X. Volume effect upon martensitic transformation in Ti<sub>29.7</sub>Ni<sub>50.3</sub>Hf<sub>20</sub> high temperature shape memory alloy [J]. Scripta Materialia, 2020, 178: 67–70.
- [7] SHUITCEV A, VASIN R N, BALAGUROV A M, LI L, BOBRIKOV I A, SUMNIKOV S V, TONG Y X. Study of martensitic transformation in TiNiHfZr high temperature shape memory alloy using in situ neutron diffraction [J]. Journal of Alloys and Compounds, 2022, 899: 163322.
- [8] REN Jia-rui, SHUITCEV A V, SUN Bin, CHEN Feng, LI Li, TONG Yun-xiang. Evolution of Ti<sub>3</sub>Ni<sub>4</sub> precipitates in Ti<sub>49.2</sub>Ni<sub>50.8</sub> alloy during equal channel angular pressing [J]. Transactions of Nonferrous Metals Society of China, 2021, 31: 980–987.
- [9] ZHANG Dian-tao, GUO Bao, TONG Yun-xiang, TIAN Bing, LI Li, ZHENG Yu-feng, GUNDEROV D V, VALIEV R Z. Effect of annealing temperature on martensitic transformation of Ti<sub>49.2</sub>Ni<sub>50.8</sub> alloy processed by equal channel angular pressing [J]. Transactions of Nonferrous Metals Society of China, 2016, 26: 448–455.
- [10] KOCKAR B, KARAMAN I, KIM J I, CHUMLYAKOV Y. A method to enhance cyclic reversibility of NiTiHf high temperature shape memory alloys [J]. Scripta Materialia, 2006, 54: 2203–2208.
- [11] SHUITCEV A V, GUNDEROV D V, SUN B, LI L, VALIEV R Z, TONG Y X. Nanostructured Ti<sub>29.7</sub>Ni<sub>50.3</sub>Hf<sub>20</sub> high temperature shape memory alloy processed by high-pressure torsion [J]. Journal of Materials Science & Technology, 2020, 52: 218–225.
- [12] REN Y, SHUITCEV A V, GUNDEROV D V, LI L, VALIEV R Z, TONG Y X. The role of temperature in the microstructural evolution of HPT-processed NiTiHf high-temperature shape memory alloy [J]. Materials Letters, 2022, 322: 132484.
- [13] BIGELOW G S, GARG A, PADULA II S A, GAYDOSH D J, NOEBE R D. Load-biased shape-memory and superelastic properties of a precipitation strengthened high-temperature Ni<sub>50.3</sub>Ti<sub>29.7</sub>Hf<sub>20</sub> alloy [J]. Scripta Materialia, 2011, 64: 725-728.
- [14] KARACA H E, SAGHAIAN S M, DED G, TOBE H, BASARAN B, MAIER H J, NOEBE R D, CHUMLYAKOV Y I. Effects of nanoprecipitation on the shape memory and material properties of an Ni-rich NiTiHf high temperature shape memory alloy [J]. Acta Materialia, 2013, 61: 7422–7431.
- [15] HAN X D, WANG R, ZHANG Z, YANG D Z. A new precipitate phase in a TiNiHf high temperature shape memory alloy [J]. Acta Materialia, 1998, 46: 273–281.
- [16] SANTAMARTA R, ARROYAVE R, PONS J, EVIRGEN A, KARAMAN I, KARACA H E, NOEBE R D. TEM study of structural and microstructural characteristics of a precipitate phase in Ni-rich Ni-Ti-Hf and Ni-Ti-Zr shape memory alloys [J]. Acta Materialia, 2013, 61: 6191–6206.
- [17] YANG F, COUGHLIN D R, PHILLIPS P J, YANG L, DEVARAJ A, KOVARIK L, NOEBE R D, MILLS M J.

- Structure analysis of a precipitate phase in an Ni-rich high-temperature NiTiHf shape memory alloy [J]. Acta Materialia, 2013, 61: 3335–3346.
- [18] KIM H Y, JINGUU T, NAM T H, MIYAZAKI S. Cold workability and shape memory properties of novel Ti–Ni–Hf–Nb high-temperature shape memory alloys [J]. Scripta Materialia, 2011, 65: 846–849.
- [19] PRASAD R V S, PARK C H, KIM S W, HONG J K, YEOM J T. Microstructure and phase transformation behavior of a new high temperature NiTiHf-Ta shape memory alloy with excellent formability [J]. Journal of Alloys and Compounds, 2017, 697: 55-61.
- [20] FAN X M, SUN S Y, TONG Y X, LI L, TIAN B, CHEN F, ZHENG Y F. Microstructure and martensitic transformation of NiTiHfSc high temperature shape memory alloys [J]. Journal of Alloys and Compounds, 2019, 779: 212–218.
- [21] TONG Y X, FAN X M, SHUITCEV A V, CHEN F, TIAN B, LI L, ZHENG Y F. Effect of Sc addition and aging on microstructure and martensitic transformation of Ni-rich NiTiHfSc high temperature shape memory alloys [J]. Journal of Alloys and Compounds, 2020, 845: 156331.
- [22] YI Xiao-yang, GAO Wei-hong, MENG Xiang-long, GAO Zhi-yong, CAI Wei, ZHAO Lian-cheng. Martensitic transformation behaviors and mechanical properties of (Ti<sub>36</sub>Ni<sub>49</sub>Hf<sub>15</sub>)<sub>100-x</sub>Y<sub>x</sub> high temperature shape memory alloys [J]. Journal of Alloys and Compounds, 2017, 705: 98–104.
- [23] YI Xiao-yang, PANG Guo-bo, SUN Bin, MENG Xiang-long, CAI Wei. The microstructure and martensitic transformation behaviors in Ti–Ni–Hf–X (Ag, Sn) high temperature shape memory alloys [J]. Journal of Alloys and Compounds, 2018, 756: 19–25.
- [24] HSU D H D, HORNBUCKLE B C, VALDERRAMA B, BARRIE F, HENDERSON H B, THOMPSON G B, MANUEL M V. The effect of aluminum additions on the thermal, microstructural, and mechanical behavior of NiTiHf shape memory alloys [J]. Journal of Alloys and Compounds, 2015, 638: 67–76.
- [25] CHASTAING K, VERMAUT P, OCHIN P, SEGUI C, LAVAL J Y, PORTIER R. Effect of Cu and Hf additions on NiTi martensitic transformation [J]. Materials Science & Engineering A, 2006, 438/439/440: 661–665.
- [26] MENG X L, CAI W, LAU K T, ZHAO L C, ZHOU L M. Phase transformation and microstructure of quaternary TiNiHfCu high temperature shape memory alloys [J]. Intermetallics, 2005, 13: 197–201.
- [27] MENG X L, FU Y D, CAI W, LI Q F, ZHAO L C. Cu content and annealing temperature dependence of martensitic transformation of Ti<sub>36</sub>Ni<sub>49-x</sub>Hf<sub>15</sub>Cu<sub>x</sub> melt spun ribbons [J]. Intermetallics, 2009, 17: 1078–1084.
- [28] MENG X L, TONG Y X, LAU K T, CAI W, ZHOU L M, ZHAO L C. Effect of Cu addition on phase transformation of Ti-Ni-Hf high-temperature shape memory alloys [J]. Materials Letters, 2002, 57: 452-456.
- [29] ACAR E, TOBE H, KAYA I, KARACA H E, CHUMLYAKOV Y I. Compressive response of Ni<sub>45.3</sub>Ti<sub>34.7</sub>Hf<sub>15</sub>Pd<sub>5</sub> and Ni<sub>45.3</sub>Ti<sub>29.7</sub>Hf<sub>20</sub>Pd<sub>5</sub> shape-memory [J]. Journal of Materials Science, 2015, 50: 1924–1934.
- [30] KARACA H E, ACAR E, DED G S, BASARAN B, TOBE H, NOEBE R D, BIGELOW G S, CHUMLYAKOV Y I.

- Shape memory behavior of high strength NiTiHfPd polycrystalline alloys [J]. Acta Materialia, 2013, 61: 5036–5049.
- [31] HONG H S, KIM J T, PARK H J, KIM Y S, SUH J Y, NA Y S, LIM K R, SHIM C H, PARK J M, KIM K B. Influence of Zr content on phase formation, transition and mechanical behavior of Ni-Ti-Hf-Zr high temperature shape memory alloys [J]. Journal of Alloys and Compounds, 2017, 692: 77–85.
- [32] HSIEH S F, WU S K. Lattice parameters of martensite in Ti<sub>50.52-x</sub>Ni<sub>49.5</sub>Zr<sub>x/2</sub>Hf<sub>x/2</sub> quaternary shape memory alloys [J]. Journal of Alloys and Compounds, 2000, 312: 288–294.
- [33] KARACA H E, ACAR E, BASARAN B, NOEBE R D, CHUMLYAKOV Y I. Superelastic response and damping capacity of ultrahigh-strength [111]-oriented NiTiHfPd single crystals [J]. Scripta Materialia, 2012, 67: 447–450.
- [34] LIN H C, LIN K M, CHANG S K, LIN C S. A study of TiNiV ternary shape memory alloys [J]. Journal of Alloys and Compounds, 1999, 284: 213–217.
- [35] YANG Hong-liang, CHEN Jian, LI Ya-hua, SHI Xiao-bin, LI Yong-tao, ZHANG Jun-song. Effect of cold work on martensitic transformation of Ni<sub>38</sub>Ti<sub>37</sub>V<sub>25</sub> alloy reinforced by V nanowires [J]. Journal of Alloys and Compounds, 2020, 815: 152489.
- [36] ZHANG J L, CANN J L, MAISEL S B, QU K, PLANCHER E, SPRINGER H, POVODEN-KARADENIZ E, GAO P, REN Y, GRABOWSKI B, TASAN C C. Design of a V-Ti-Ni alloy with superelastic nano-precipitates [J]. Acta Materialia, 2020, 196: 710-722.
- [37] LUTTEROTTI L, MATTHIES S, WENK H R, SCHULTZ A S, RICHARDSON J W. Combined texture and structure analysis of deformed limestone from time-of-flight neutron diffraction spectra [J]. Journal of Applied Physics, 1997, 81: 594–600.
- [38] SHUITCEV A V, TONG Yun-xiang, LI Li. Indentation size effect and strain rate sensitivity of Ni<sub>3</sub>Ta high temperature shape memory alloy [J]. Vacuum, 2019, 160: 25–30.
- [39] SHUITCEV A V, REN Yi, SUN Bin, MARKOVA G V, LI Li, TONG Yun-xiang, ZHENG Yu-feng. Precipitation and coarsening kinetics of *H*-phase in NiTiHf high temperature shape memory alloy [J]. Journal of Materials Science & Technology, 2022, 114: 90–101.
- [40] HORNBUCKLE B C, SASAKI T T, BIGELOW G S, NOEBE R D, WEAVER M L, THOMPSON G B. Structure–property relationships in a precipitation strengthened Ni–29.7Ti–20Hf (at.%) shape memory alloy [J]. Materials Science and Engineering A, 2015, 637: 63–69.
- [41] KORNEGAY S M, KAPOOR M, HORNBUCKLE B C, TWEDDLE D, WEAVER M L, BENAFAN O, BIGELOW G B, NOEBE R D, THOMPSON G B. Influence of *H*-phase precipitation on the microstructure and functional and mechanical properties in a Ni-rich NiTiZr shape memory alloy [J]. Materials Science and Engineering A, 2021, 801: 140401.
- [42] MOSHREF-JAVADI M, SEYEDEIN S H, SALEHI M T, ABOUTALEBI M R. Age-induced multi-stage transformation in a Ni-rich NiTiHf alloy [J]. Acta Materialia, 2013, 61: 2583–2594.
- [43] RÖNNEBRO E, NORÉUS D, TSUKAHARA M, SAKAI S.

- Neutron diffraction study of the new hexagonal Laves phase  $(Hf,Ti)(Ni,V)_2$  and its deuteride [J]. Journal of Alloys and Compounds, 1999, 293/294/295: 169-173.
- [44] ZOU Lei, GUO Cui-ping, LI Chang-rong, DU Zhen-min. Experimental investigation and thermodynamic modeling of the Ni-Ti-V system [J]. Calphad, 2019, 64: 97–114.
- [45] CHEN Sinn-wen, HO Chun-sheng, LIN Chin-hao, CHEN Chin-ming. The 900 °C isothermal section of Ti-Ni-V alloys [J]. Metallurgical and Materials Transactions A, 2000, 31: 1679–1682.
- [46] LE BAIL A, DUROY H, FOURQUET J L. Ab-initio structure determination of LiSbWO<sub>6</sub> by X-ray powder diffraction [J]. Materials Research Bulletin, 1988, 23: 447–452.
- [47] YI Xiao-yang, SUN Bin, GAO Wei-hong, MENG Xiang-long, GAO Zhi-yong, CAI Wei, ZHAO Lian-cheng. Microstructure evolution and superelasticity behavior of Ti-Ni-Hf shape memory alloy composite with multi-scale and heterogeneous reinforcements [J]. Journal of Materials Science & Technology, 2020, 42: 113-121.
- [48] YI Xiao-yang, SUN Bin, SUN Kui-shan, WANG Hai-zhen, ZHANG Shang-zhou, GAO Zhi-yong, MENG Xiang-long. Revealing the interface structure of {111} type I twin in Ti-Ni-Hf shape memory alloy composite [J]. Journal of Materials Science & Technology, 2022, 105: 237–241.
- [49] SHUITCEV A V, TONG Yun-xiang, WANG Yu, CONG Dao-yong. Polycrystalline shape-memory alloy and strain glass [M]. Singapore: Springer Singapore, 2022.

- [50] LIU J L, ZHU L L, HUANG X M, CAI G M, JIN Z P. Investigation of the phase equilibria in Ti–Ni–Hf system using diffusion triples and equilibrated alloys [J]. Calphad, 2017, 58: 160–168.
- [51] ZHAO Xin-qing, YAN Xiao-ming, YANG Ya-zhuo, XU Hui-bin. Wide hysteresis NiTi(Nb) shape memory alloys with low Nb content (4.5 at.%) [J]. Materials Science and Engineering A, 2006, 438/439/440: 575–578.
- [52] EVIRGEN A, KARAMAN I, SANTAMARTA R, PONS J, HAYRETTIN C, NOEBE R D. Relationship between crystallographic compatibility and thermal hysteresis in Ni-rich NiTiHf and NiTiZr high temperature shape memory alloys [J]. Acta Materialia, 2016, 121: 374–383.
- [53] SHUITCEV A V, KHOMUTOV M G, VASIN R N, LI L, GOLOVIN I S, ZHENG Y F, TONG Y X. The role of H-phase in thermal hysteresis and shape memory properties in Ni<sub>50</sub>Ti<sub>30</sub>Hf<sub>20</sub> alloy [J]. Scripta Materialia, 2023, 230: 115391.
- [54] SAGHAIAN S M, KARACA H E, SOURI M, TURABI A S, NOEBE R D. Tensile shape memory behavior of Ni<sub>50.3</sub>Ti<sub>29.7</sub>Hf<sub>20</sub> high temperature shape memory alloys [J]. Materials & Design, 2016, 101: 340–345.
- [55] KARACA H, ACAR E, DED G S, SAGHAIAN S M, BASARAN B, TOBE H, KOK M, MAIER H J, NOEBE R D, CHUMLYAKOV Y I. Microstructure and transformation related behaviors of a Ni<sub>45.3</sub>Ti<sub>29.7</sub>Hf<sub>20</sub>Cu<sub>5</sub> high temperature shape memory alloy [J]. Materials Science and Engineering A, 2015, 627: 82–94.

# 四元 NiTiHfV 合金的显微组织与马氏体相变

Aleksandr V. SHUITCEV<sup>1</sup>, 任 艺<sup>1</sup>, 张泽中<sup>1</sup>, Roman N. VASIN<sup>2</sup>, 孙 斌<sup>3</sup>, 李 莉<sup>1</sup>, 佟运祥<sup>1</sup>

- 1. 哈尔滨工程大学 材料科学与化学工程学院 黑龙江省先进纳米材料联合实验室(国际合作),哈尔滨 150001;
  - 2. Frank Laboratory of Neutron Physics, Joint Institute for Nuclear Research, 141980, Dubna, Russia;
    - 3. 哈尔滨工程大学 材料科学与化学工程学院 分析测试中心,哈尔滨 150001
- **摘 要**:利用扫描电子显微观察、透射电子显微观察、X 射线衍射分析、差示扫描量热分析、硬度测试和弯曲测试研究了(NisoTisoHf2o)95V5 合金的显微组织、马氏体相变行为与形状记忆性能。结果表明,添加 V 可显著影响合金的显微组织。添加 V 会导致合金中形成室温下与 B19'马氏体相共存的(Ni,V)2(Ti,Hf)型 Laves 相。经 550 °C 时效处理的合金表现出析出强化行为,这主要是因为合金中形成纳米尺寸的正交结构的 H 相。当时效时间为 3 h 时,合金表现出峰值硬度。与固溶态合金相比,时效态合金表现出较大的相变应变和较小的不可恢复应变,当外加应力为 500 MPa 时,合金达到最大相变应变,为 1.56%。

关键词:形状记忆合金; NiTiHfV; H相; Laves 相; 马氏体相变

(Edited by Bing YANG)